Free Radical Biology and Medicine 152 (2020) 336–347

Contents lists available at ScienceDirect

Free Radical Biology and Medicine

journal homepage: www.elsevier.com/locate/freeradbiomed

Original article

2-Methoxy-6-acetyl-7-methyljuglone (MAM) induced programmed necrosis in glioblastoma by targeting NAD(P)H: Quinone oxidoreductase 1 (NQO1)

Jie Yu[a], Bingling Zhong[a], Long Jin[b,c], Ying Hou[a], Nana Ai[d], Wei Ge[d], Luoxiang Li[e], Shuqin Liu[e], Jin-Jian Lu[a], Xiuping Chen[a,*]

[a] State Key Laboratory of Quality Research in Chinese Medicine, Institute of Chinese Medical Sciences, University of Macau, Taipa, Macau, China
[b] Shengli Clinical Medical College, Fujian Medical University, Fuzhou, 350001, China
[c] Department of Pathology, Fujian Provincial Hospital, No.134 Dong Street, Fuzhou, 350001, China
[d] Centre of Reproduction, Development and Aging (CRDA), Faculty of Health Sciences, University of Macau, Taipa, Macau, China
[e] Hospital of Chengdu University of Traditional Chinese Medicine, Chengdu, 610072, China

ARTICLE INFO

Keywords:
MAM
Glioblastoma
Programmed necrosis
NQO1

ABSTRACT

Glioblastoma (GBM) are the most malignant brain tumors in humans and have a very poor prognosis. Temozolomide (TMZ), the only chemotherapeutic drug for GBM treatment, induced apoptosis but frequently developed resistance. Non-apoptotic cell death offers an alternative strategy to fight cancers. Our previous studies showed that 2-methoxy-6-acetyl-7-methyljuglone (MAM), a natural product, induced necroptosis in lung and colon cancer cells. The current study is designed to investigate its therapeutic potentials for GBM with *in vitro* and *in vivo* models. The protein expression of NAD(P)H: quinone oxidoreductase 1 (NQO1) in human GBM specimens were detected by immunohistochemistry. Effect of MAM on NQO1 was measured by recombinant protein and cellular thermal shift assay. The roles of NQO1 activation, superoxide (O_{2^-}) generation, calcium (Ca^{2+}) accumulation, and c-Jun N-terminal kinase (JNK1/2) activation in MAM-induced cell death in U87 and U251 glioma cells were investigated. The effect of MAM on tumor growth was tested with a U251 tumor xenograft zebrafish model. Results showed that the NQO1 expression is positively correlated with the degree of malignancy in GBM tissues. MAM could directly bind and activate NQO1. Furthermore, MAM treatment induced rapid O_{2^-} generation, cytosolic Ca^{2+} accumulation, and sustained JNK1/2 activation. In addition, MAM significantly suppressed tumor growth in the zebrafish model. In conclusion, MAM induced GBM cell death by triggering an O_{2^-}/Ca^{2+}/JNK1/2 dependent programmed necrosis. NQO1 might be the potential target for MAM and mediated its anticancer effect. This non-apoptotic necrosis might have therapeutic potentials for GBM treatment.

1. Introduction

Glioblastoma (GBM) is the most common and aggressive type of primary malignant brain tumor, classified as high-grade IV glioma by the World Health Organization (WHO). The average survival is no longer than one year, even though the patients accepted surgery in combination with postoperative radiotherapy and chemotherapy [1]. Temozolomide (TMZ) is the primary systemic chemotherapy agent used in the treatment of GBM [2]. However, TMZ cause cognitive impairment due to normal brain cell damage, and higher doses of TMZ are proscribed due to dose-limiting bone marrow suppression with severe leukopenia and thrombocytopenia. Moreover, resistance to apoptosis is associated with poor prognosis to currently used chemotherapy and radiotherapy [3]. Elucidation of novel cell death pathways for killing glioma cells may lead to more effective treatment strategies.

NAD(P)H: quinone oxidoreductase 1 (NQO1, EC 1.6.99.2) is a two-electron oxidoreductase involved in phase II detoxifying reactions [4]. NQO1 can catalyze and revert of a wide variety of compounds, including quinones nitroaromatic compounds, imidazoles and iron (III) ions [5]. NQO1 is highly expressed in most human solid tumors, including colon cancer, breast cancer, pancreas cancer, liver cancer and lung cancer [6–9]. Particularly, the expression of NQO1 was enhanced in GBM cell lines, which may be a priority target of GBM [10]. Notably, several NQO1 bioactivatable quinones such as β-Lapachone [11], and deoxynyboquinones [12], showed significant anticancer effect. Especially, β-Lapachone and its analogs have been in clinical trials for the treatment of cancer [11,13–15].

Our previous studies showed that 2-methoxy-6-acetyl-7-

* Corresponding author. Institute of Chinese Medical Sciences, University of Macau, Avenida da Universidade, Taipa, Macau, China.
E-mail address: xpchen@um.edu.mo (X. Chen).

https://doi.org/10.1016/j.freeradbiomed.2020.03.026
Received 8 January 2020; Received in revised form 24 March 2020; Accepted 24 March 2020
Available online 28 March 2020
0891-5849/

Abbreviations

Ca^{2+}	calcium
CaMKII	calcium-calmodulin dependent protein kinase II
DHE	dihydroethidium
DIC	dicoumarol
DiI	1,1′-dioctadecyl-3,3,3′,3′-tetramethylindocarbocyanine perchlorate
DMSO	dimethyl sulfoxide
DTT	dithiothreitol
EGTA	ethylene glycol tetraacetic acid
GBM	glioblastoma
GSH	glutathione
hpf	hour post-fertilization
JC-1	5,5′,6,6′-tetrachloro-1,1′,3,3′- tetraethylbenzimidazolyl-carbocyanine iodide
JNK1/2	c-Jun N-terminal kinase 1/2
MAM	2-methoxy-6-acetyl-7-methyljuglone
ΔΨm	mitochondrial membrane potential
NAC	N-acetyl-L-cysteine
NQO1	NAD(P)H: quinone oxidoreductase 1
O_{2^-}	superoxide
PI	propidium iodide
PTU	1-phenyl-2-thiourea
ROS	reactive oxygen species
SiRNA	small interfering RNA
TMRM	tetramethylrhodamine methyl ester
TMZ	temozolomide
TCGA	the Cancer Genome Atlas
WHO	world health organization
Z-VAD-fmk	benzyloxycarbonyl-Val-Ala-Asp (OMe) fluoromethylk-etone

methyljuglone (MAM), a natural naphthoquinone, induced necroptosis in lung and colon cancer cells [16–18]. Given its ability to cross the blood-brain barrier [19], it is of interest to test its effect on GBM. Here, we showed that MAM triggered a unique NQO1-dependent programmed necrosis in GBM cells, which might provide novel therapeutic potentials to combat GBM.

2. Materials and methods

2.1. Cells and reagents

U87 and U251 cells purchased from Cell Bank of Type Culture Collection of Chinese Academy of Sciences (Shanghai, China) were cultured in DMEM with 10% FBS and 1% PS at 37 ˚C in a humidified environment with 5% CO_2. MAM (> 97%) was purified from the dried rhizome of *P. cuspidatum* as our previous report [16]. Dihydroethidium (DHE), Fluo-3AM ester, tetramethylrhodamine methyl ester (TMRM), Hoechst 33342, Propidium iodide (PI) and BAPTA-AM were purchased from Molecular Probes (Eugene, OR, USA). N-acetyl-L-cysteine (NAC), ethylene glycol tetraacetic acid (EGTA) and SP600125 were purchased from Sigma Aldrich (St Louis, MO, USA). Dicoumarol (DIC), KN93 and benzyloxycarbonyl-Val-Ala-Asp (OMe) fluoromethylketone (Z-VAD-fmk) were purchased from Selleckchem (Houston, TX, USA). Glutathione (GSH), catalase, dithiothreitol (DTT) and 5,5′,6,6′-tetrachloro-1,1′,3,3′- tetraethylbenzimidazolylcarbocyanine iodide (JC-1) were purchased from Beyotime (Shanghai, China). 1,1′-dioctadecyl-3,3,3′,3′-tetramethylindocarbocyanine perchlorate (DiI) and Mitosox Red were purchased from Invitrogen (Carlsbad, CA, USA). Antibodies for GAPDH (5174S), p-JNK1/2 (4668S), JNK1/2 (9252S), p-CaMKII (12716S), NQO1 (3187S), HMGB1 (3935s) and horseradish peroxidase-conjugated secondary antibodies (7074 V) were purchased from Cell Signaling Technology (Beverly, MA, USA).

2.2. NQO1 activity assay

NQO1 activity assay was performed as previously described [20,21]. Briefly, NQO1 enzymatic activity was measured using the decrease in NADH absorbance at 340 nm with a FlexStation 3 microplate reader (Molecular Devices, Sunnyvale, CA). The reaction mixture in a final volume of 200 μL containing 50 μg of cell extracts or 50 ng of recombinant NQO1 protein (BioVision, Milpitas, CA, USA), 5 μM FAD, 200 μM NADH and Tris-HCl buffer (25 mM Tris-HCl, pH 7.5, 0.7 mg/mL BSA, 0.01% Tween 20).

2.3. Cellular thermal shift assay

Cellular thermal shift assay (CETSA) was performed as previously described [22,23]. Briefly, cell extracts were prepared and treated with MAM or dimethyl sulfoxide (DMSO) for 1 h at room temperature. Each sample was aliquoted into 7 tubes and then heated at indicated temperature for 5 min using an Eppendorf Thermomixer with gentle mixing. Subsequently, cell lysates were centrifuged at 15,000 rpm for 20 min at 4 ˚C, and then the supernatant was analyzed by Western blotting. For quantitation, band intensities were normalized to the mean of the lowest temperature bands, in which protein levels stayed constant.

2.4. Molecular docking

The NQO1 crystal structure was obtained from RCSB Protein Data Bank (PDB ID: 2F1O) [24]. MAM was drawn by ChemDraw and minimized the energy by Chem3D. The NQO1 and MAM was docked with AutoDock 4.2 [25]. AutoDockTools were used to prepare the protein and ligand. .The docking results were visualized by Chimera 1.13.1 [26].

2.5. Cell viability assay

The LDH release was determined with an LDH assay kit (Beyotime Biotech, Nanjing, China) following the manufacturer's instructions.

2.6. Western blotting

After the cell lysates and whole-zebrafish lysates were prepared and collected, the protein contents were determined by BCA protein assay kit (Pierce Biotechnology). Then equal amount of protein from each sample was separated by SDS/PAGE gel electrophoresis and transferred to PVDF membranes. Signals of chemiluminescence intensity were acquired using a ChemiDoc™ MP Imaging System and analyzed with Image Lab software (Bio-Rad, Hercules, CA, USA) as previously described [16,17].

2.7. Transfection of small interfering RNA (siRNA)

For siRNA knockdown, cells were transfected with indicated siRNAs by using Lipofectamine 3000 (Invitrogen, Carlsbad, CA, USA) according to the manufacturer's introductions. The NQO1 siRNA (5′-GAACCUCA ACUGACAUAUA-3′) and Scrambled siRNA were purchased from Genepharma Company (Shanghai, China).

2.8. Caspase activity assay

The caspase 3/7, 8 and 9 activities were determined using Caspase-Glo Assay Kits (Promega, Madison, WI, USA) according to the

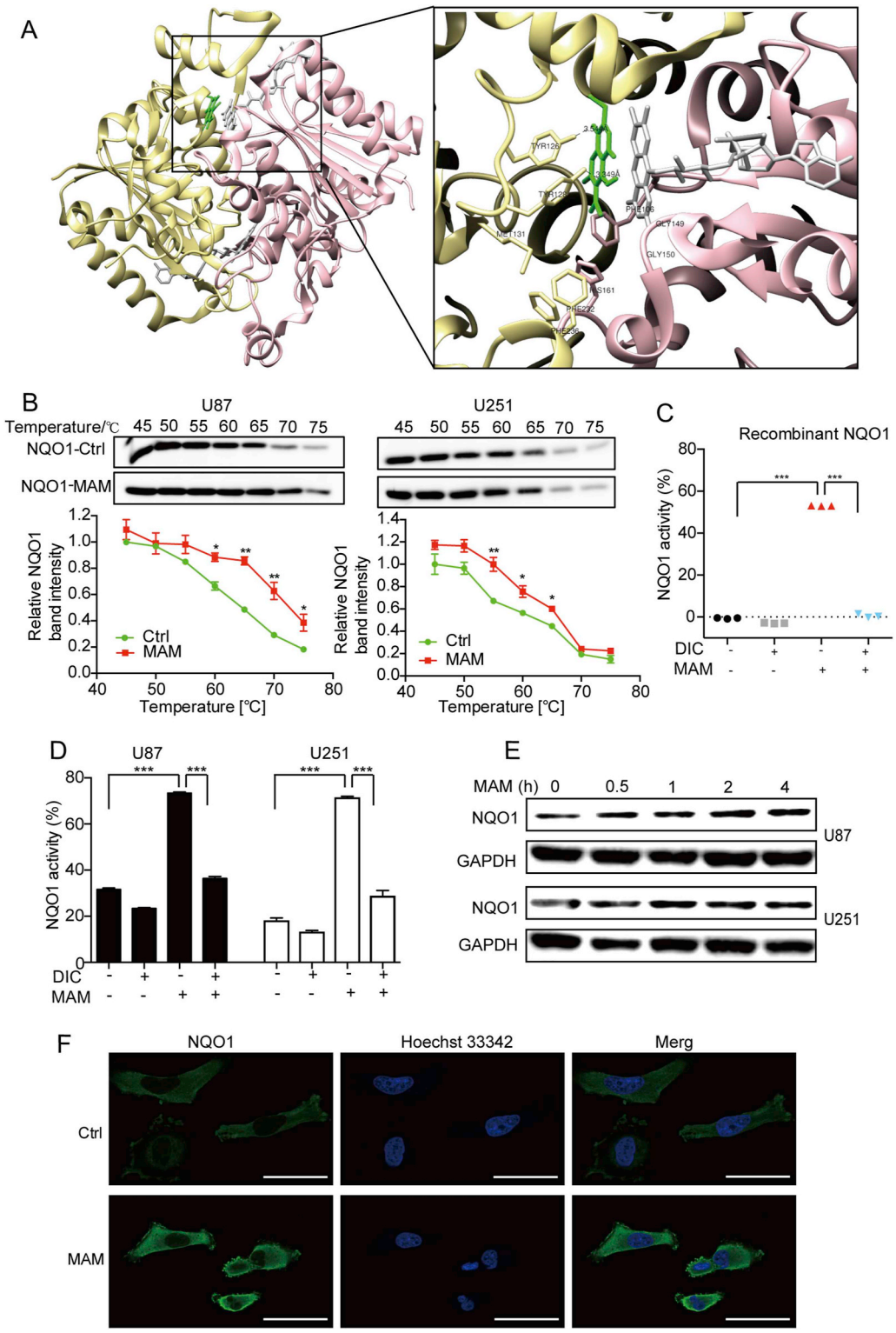

Fig. 1. MAM is an NQO1 substrate. (A) Binding mode of MAM in NQO1 crystalline structures obtained with a molecular docking calculation. Close-up view of the interaction between MAM and surrounding residues in NQO1 is shown in the right panel. NQO1 chains B is represented by a yellow cartoon and chains D is pink. MAM (green), FAD (gray) and the residues in the active binding site are shown in sticks. (B) MAM interacts with NQO1 in GBM cell lines. Western blotting image and the cellular thermal shift assay curves show that MAM increased the thermal stability of NQO1 protein in both U87 and U251 cells. Data are represented as means ± SD, n = 3 independent experiments, $*p < 0.05$, $**p < 0.001$. (C) MAM increases NQO1 enzymatic activity *in vitro*. Enzymatic activity of recombinant NQO1 was determined in the absence or presence of DIC. (D) MAM increases NQO1 enzymatic activity in GBM cells. NQO1 activity was determined in cell extracts prepared from U87 and U251 cells. (E) Cells were treated with MAM, protein expression was determined by Western blotting analysis. (F) U251 cells were treated with or without MAM treatment for 2 h, NQO1 expression was visualized using immunofluorescence staining. Image were captured with a confocal microscope. Bar = 50 μm. (For interpretation of the references to colour in this figure legend, the reader is referred to the Web version of this article.)

manufacturer's instructions.

2.9. Annexin V/7AAD double staining

Flow cytometry with human Annexin V (PE)/7AAD (BD Biosciences, San, Jose, CA, USA) double staining was used to distinguish apoptosis and necrosis. Briefly, after treatment of MAM, cells were harvested at the indicated time points followed by incubation with Annexin V/7AAD solution for 15 min at room temperature in the dark. The samples were immediately analyzed by flow cytometry using a FACSanto™ system (BD Biosciences).

2.10. PI staining assay

The PI staining was performed as a previous report [27]. After treatment with MAM, cells were incubated with PI (5 μg/mL) for 15 min at room temperature. Images were captured using an inverted fluorescent microscope Olympus IX73 (Olympus Corporation, Tokyo,

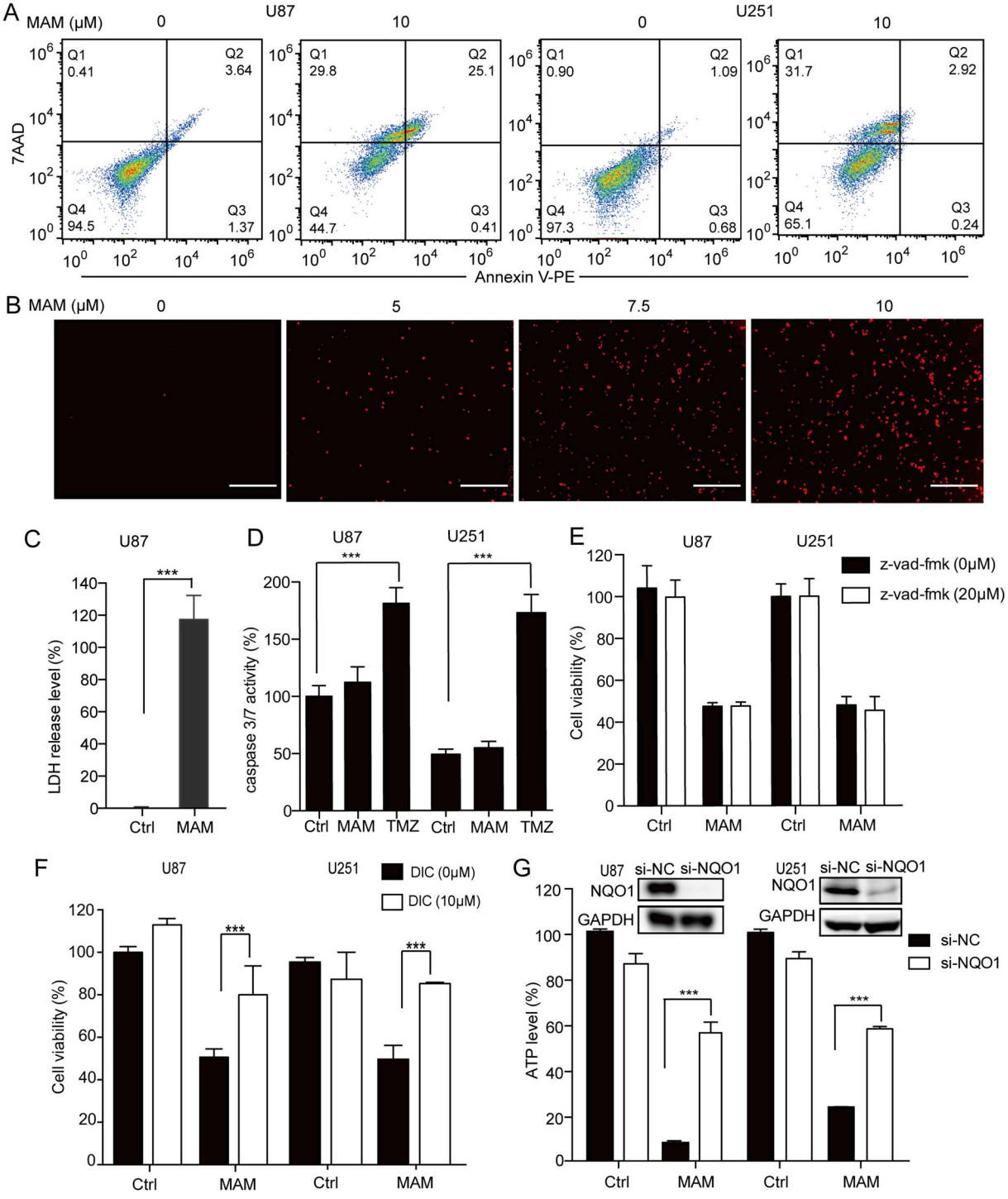

Fig. 2. MAM induced NQO1-dependent non-apoptotic cell death. (A) MAM induced non-apoptotic cell death in GBM cells. Cells were treated with MAM for 8 h, the cell death was detected with Annexin V-PE/7AAD double staining by flow cytometry. (B) PI staining analysis of MAM treated GBM cells. Cells were treated with MAM for 8 h, and then stained with PI. Images were capture using a fluorescence microscope. Bar = 200 μm. (C) LDH release was determined using an LDH assay kit after MAM treatment on U87 cells for 8 h. (D) Caspase 3/7 activities were determined using Caspase-Glo Assay Kit after MAM or TMZ treatment on GBM cells. TMZ was the positive control. (E) U87 and U251 cells were treated with Z-VAD-fmk (20 μM) for 1 h, followed by MAM treatment for another 8 h. Cell viability was measured by MTT assay. **(**F) The MTT assay evaluating the effect of NQO1 inhibitor DIC on MAM-induced GBM cell death. Cells were treated with MAM for 8 h in the presence or absence of DIC pretreatment for 1 h. Cell viability was measured by MTT assay. (G) Effects of NQO1 knockdown on MAM-induced GBM cell death. Cells were transfected with siRNA of NQO1 or NC (Negative Control) and then treated with MAM for 8 h. Cell viabilities were evaluated by ATP assay. Error bars represent standard deviations of the separate experiments. ***$p < 0.001$, analyzed by one-way ANOVA with Dunnett's *post hoc* test.

Japan).

2.11. Measurement of intracellular superoxide (O_{2^-})

After treatment with MAM at different time points with or without inhibitors, the average level of intracellular O_{2^-} was evaluated by using the fluorescent probe DHE. All the samples were stained in the dark for 30 min with DHE (10 μM). The fluorescence was analyzed immediately by FACScanto™ flow cytometer (BD Biosciences) using the PE channel.

2.12. Measurement of intracellular calcium (Ca^{2+})

Measurement of calcium by Fluo-3AM was performed as our previous report [17]. Treated cells were incubated with 5 μM Fluo-3AM ester at 37 °C for 30 min. The fluorescence was analyzed immediately by FACScan™ flow cytometer (BD Biosciences) using the FITC channel.

2.13. Measurement of mitochondrial membrane potential ($\Delta\Psi m$)

Treated cells were stained with JC-1 (2 μg/mL) at 37 °C for 30 min in the dark and images were acquired with IN Cell Analyzer 2000 (GE Healthcare, Little Chalfont, Buckinghamshire, UK). Besides, the ΔΨm was further detected with TMRM (100 nM), incubated at 37 °C for 30 min, followed by flow cytometry analysis using the PE channel.

2.14. MitoSox red staining

To determine the mitochondrial O_{2^-} levels, cells were loaded with MitoSox Red (5 μM) at 37 °C for 30 min after MAM insults in the presence or absence of various inhibitors, followed by flow cytometry analysis using the PE channel.

2.15. Zebrafish xenograft model

Wild type zebrafish were used to establish U251-derived xenograft zebrafish model in this study. Zebrafish were maintained according to standard procedures. 2 h post-fertilization (hpf), larvae were treated with PTU (1-phenyl-2-thiourea, 0.2 mM) to remain transparent for microscopic analysis. 48 hpf larvae were anesthetized with 0.003% tricaine (Sigma, St Louis, MO, USA) and positioned on a 10 cm dish coated with 3% agarose. U251 cells were labeled with DiI (Invitrogen, Carlsbad, CA, USA) according to previously reported [28]. Cell suspensions were microinjected into 48 hpf larvae by a Nanoject II auto-Nanoliter Injector (Drummond Scientific Company, Broomall, PA) with an injection volume 4.6 nL. Approximately 200 cells were injected into the yolk sac of larvae, which were then maintained in fish water/PTU with Penicillin/Streptomycin (1:100) at 28 °C. After injection after 24 h, zebrafish were treated with MAM or TMZ for 3 days. Images were captured at 0- and 3-day time points post-injection using a fluorescent microscope (SMZ18, Nikon, Tokyo, Japan). All experiments were approved by the Animal Research Ethics Committee of the University of Macau.

2.16. Statistical analysis

All data represent at least 3 independent experiments and are expressed as Means ± SD. Statistical comparisons were made using one-way analysis of variance (ANOVA) followed by Dunnett's *post hoc* test. *P*-values of less than 0.05 were considered to represent statistical significance.

3. Results

3.1. GBM showed increased expression of NQO1

ONCOMINE analysis revealed that NQO1 mRNA expression was significantly higher in GBM patients' tissues than normal samples across a wide variety of datasets in GBM cancer type. NQO1 transcripts were increased 2.8 folds in GBM samples versus normal tissues in a dataset with 31 samples derived from the Cancer Genome Atlas (TCGA) database (Supplementary Fig. 1D). Immunohistochemical analyses confirmed the increased protein expression of NQO1 in GBM specimens (Supplementary Fig. 1A). Pathology-assisted dissection of tumor compared with associated normal tissue from different grade glioma patients confirmed elevated NQO1 expression levels in tumors compared with normal tissues (Supplementary Fig. 1B). Besides, compared with stage II, NQO1 showed a significantly higher level of expression in GBM advanced clinical stages (stage III-IV) (Supplementary Fig. 1C).

3.2. MAM activated NQO1 in GBM cells

Molecular docking analysis showed that MAM could be buried in the activation pocket of NQO1. The plane of MAM paralleled to the isoalloxazine ring of the NQO1 that forms one side of the catalytic pocket. In this pocket, it interacts with NQO1 monomers and FAD through a series of hydrophobic and hydrogen bonds. MAM formed hydrogen bonds with residues TYR126, TYR128 and could enhance the binding stability (Fig. 1A). CETSA assay revealed that MAM treatment could enhance the stability of NQO1 protein (Fig. 1B). Furthermore, MAM increased NQO1 activity in *in vitro* assay using purified recombinant NQO1. Co-treatment with DIC, an NQO1 inhibitor, suppressed NQO1 activity almost to basal level (Fig. 1C). Similar results were obtained with cellular extracts prepared from glioma cells (Fig. 1D). Interestingly, NQO1 protein expression was also upregulated by MAM (Fig. 1E and F).

3.3. MAM-induced NQO1 dependent non-apoptotic necrosis

Cytotoxicity assay showed that MAM treatment dramatically decreased the cell viability of both line cells in concentration- and time-dependent manners (Supplementary Figs. 2A and 2B). The cellular ATP levels dropped rapidly in concentration-dependent manners in both line cells as well (Supplementary Fig. 2C), while TMZ, the only clinical agent available for glioma treatment, showed no effect on ATP level (Supplementary Fig. 2F). A significant reduction in colony formation in MAM treated glioma cells was observed (Supplementary Fig. 2D). MAM treatment increased percentages of 7AAD positive cells in Annexin V/7AAD double staining (Fig. 2A). Increased PI penetration and LDH release were observed in MAM treated cells (Fig. 2B and C). MAM treatment showed no effect on cleavage of caspases 3, 7, and 9 (Supplementary Fig. 2H) and caspase 3/7, 8 and 9 activities (Fig. 2D and Supplementary Fig. 2G). In contrast, the caspase 3/7 activities were significantly increased in TMZ treated cells (Fig. 2D). Z-VAD-fmk showed no effect on MAM-induced cell death (Fig. 2E). Both silence NQO1 by siRNA and inhibition its activity by DIC significantly reversed MAM-induced cell death (Fig. 2F and G).

3.4. MAM-induced programmed necrosis via O_{2^-}

MAM treatment triggered significant intracellular O_{2^-} generation in a time-dependent manner in both cell lines (Fig. 3A). Co-treatment of NAC, a reactive oxygen species (ROS) scavenger, effectively inhibited MAM-induced O_{2^-} formation (Fig. 3B), cytotoxicity, and morphological features (Fig. 3C, D and E). Similarly, GSH, catalase, or DTT pretreatment completely reversed MAM-induced cell death (Fig. 3F, G, and H). MAM-induced O_{2^-} could also be significantly reversed by DIC pretreatment (Fig. 3I).

3.5. MAM-induced programmed necrosis via O_{2^-} mediated cytosolic Ca^{2+}

A remarkable increase in the cytosolic Ca^{2+} accumulation was observed after MAM treatment (Fig. 4A), which was further confirmed by

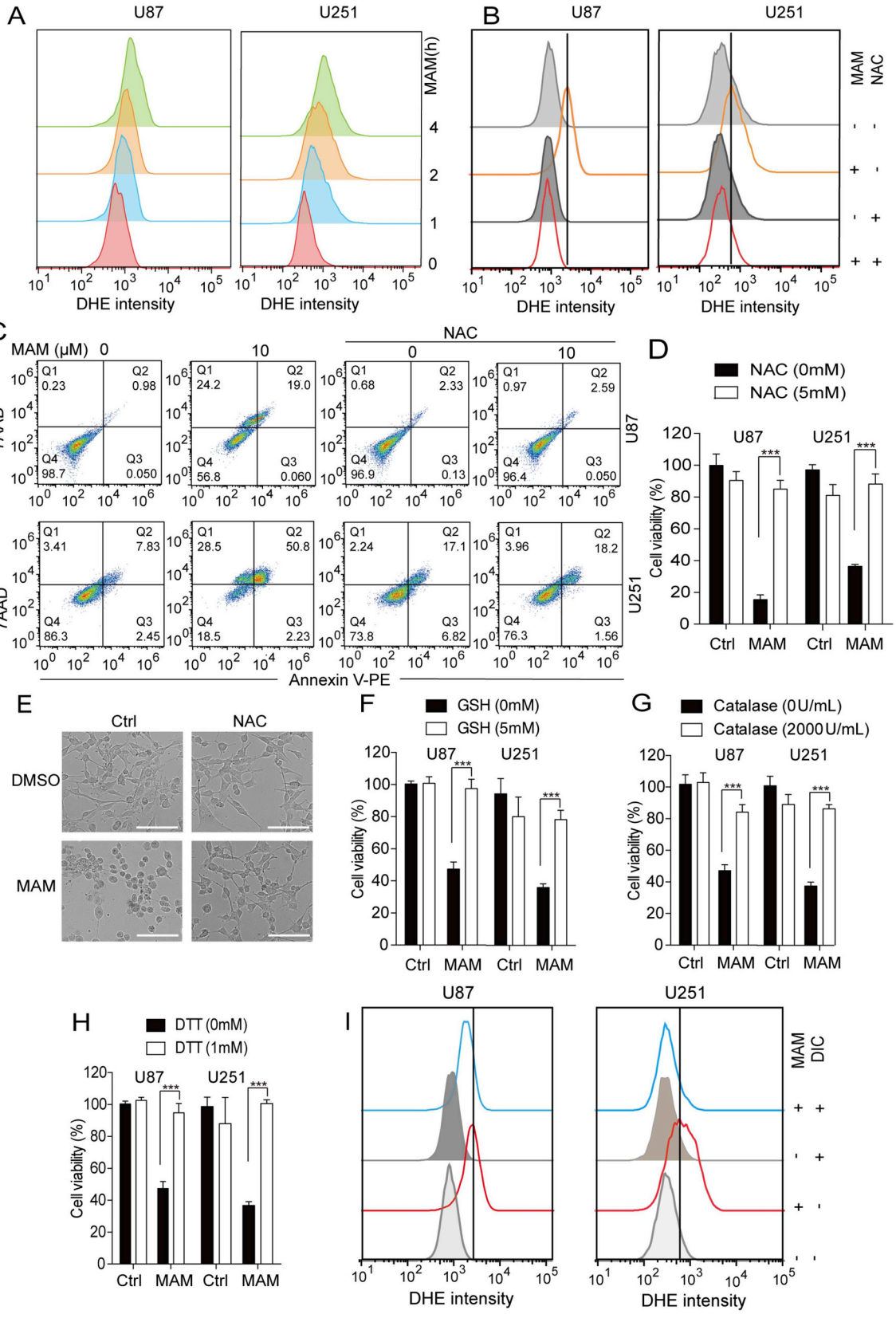

Fig. 3. MAM induced programmed necrosis via O_{2^-}. (A) Time response analysis of MAM treatment on O_{2^-} generation. Cells were treated with MAM for the indicated time and then stained with DHE probe and analysis by flow cytometry. (B) Effect of NAC on MAM-induced O_{2^-} generation. Cells were treated with MAM for 4 h in the presence or absence of NAC pretreatment for 1 h, followed by DHE staining and flow cytometry analysis. (C, D and E) Effects of NAC on MAM induced GBM cell death. Cells were pretreated with NAC for 1 h, followed by MAM treatment for 8 h. MTT assay (C), Annexin V/7AAD double staining assay (D) and morphological change (E) were used to evaluate cell viability. Bar = 100 m. (F, G, and H) Effects of different ROS inhibitors on MAM induced cell death. Cells were pretreated with GSH, catalase and DTT, followed treated with MAM for another 8 h, then the cell viability was determined by MTT assay. (I) Effect of DIC on MAM-induced O_{2^-} generation. Cells were treated with MAM for 4 h with or without DIC pretreatment for 1 h and then stained with DHE probe before flow cytometry analysis. Error bars represent standard deviations of the separate experiments. ***$p < 0.001$, analyzed by one-way ANOVA with Dunnett's *post hoc* test.

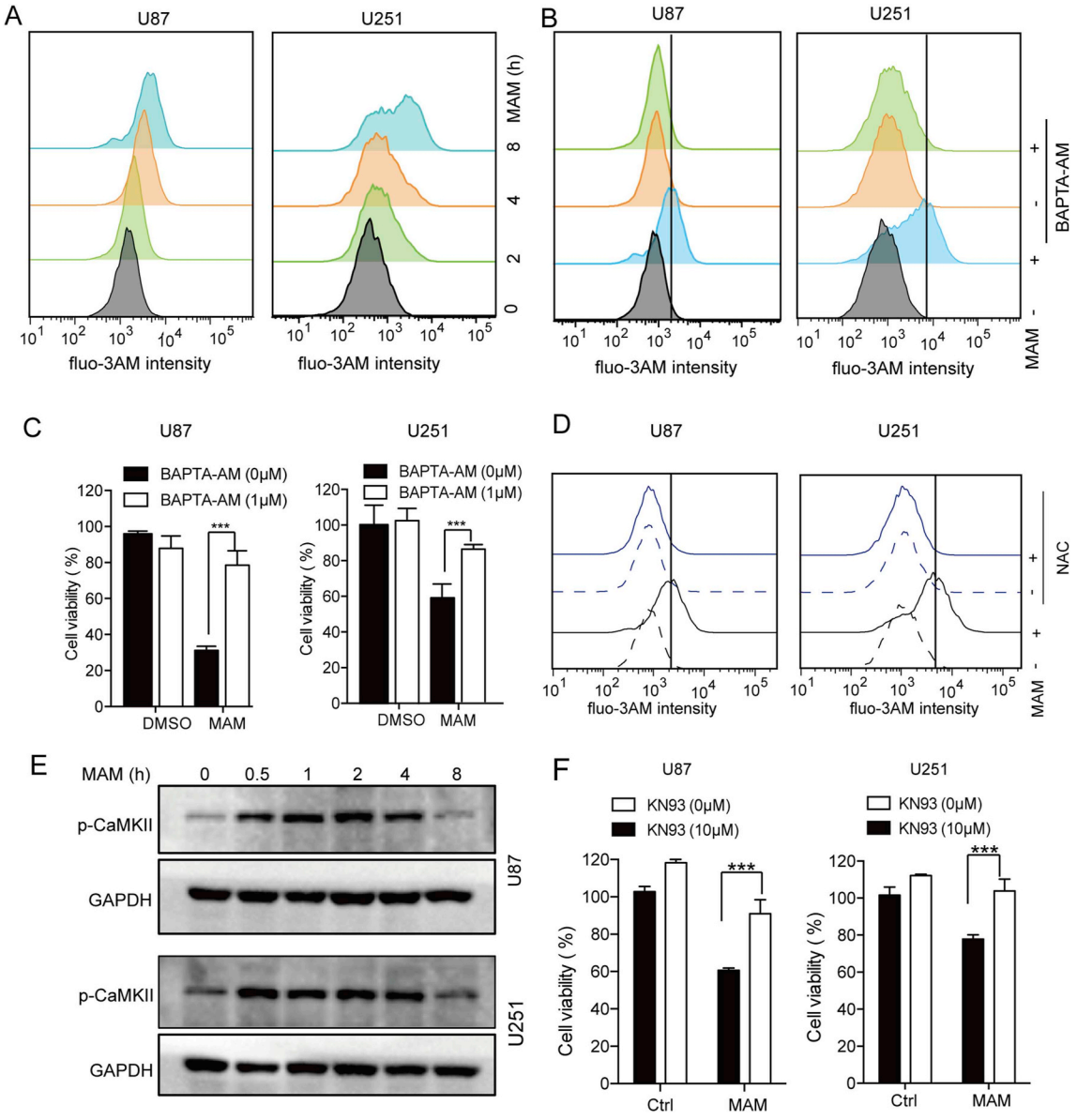

Fig. 4. MAM induced cytosolic Ca^{2+} accumulation is essential for cell death. (A) Time response analysis of MAM on Ca^{2+} concentrations indicated with Fluo-3AM fluorescence intensity by flow cytometry. Cells were treated with MAM for 2 h, 4 h or 8 h, followed by Fluo-3AM staining and flow cytometry. (B) Effects of Ca^{2+} chelator BAPTA-AM on MAM-induced Ca^{2+} elevation. Cells were pretreated with BAPTA-AM for 1 h and then exposure for MAM for another 8 h, followed by Fluo-3AM staining and flow cytometry analysis. (C) Effect of BAPTA-AM on MAM-induced cell death. Cells were treated with MAM for 8 h in the presence or absence of BAPTA-AM pretreatment for 1 h, and then cell viability was determined by MTT assay. (D) Effect of NAC on MAM-induced Ca^{2+} accumulation. Cells were treated with MAM for 8 h with or without NAC pretreatment for 1 h, followed by Fluo-3AM staining and flow cytometry analysis. (E) Western blotting analysis evaluating the expression of p-CaMKII protein in MAM treated cells for different time. GAPDH is used as a loading control. (F) Effect of CaMKII inhibitor KN93 on MAM-induced cell death. Cells were treated with MAM for 8 h in the presence or absence of KN93 pretreatment for 1 h, and then cell viability was determined by MTT assay. Error bars represent standard deviations of the separate experiments. ***$p < 0.001$, analyzed by one-way ANOVA with Dunnett's *post hoc* test.

GCaMP3 (Supplementary Figs. 3A), a genetically encoded calcium indicator [29]. Pretreatment with BAPTA-AM, a permeable Ca^{2+} chelating agent, and NAC blocked MAM-induced Ca^{2+} accumulation (Fig. 4B and D). Furthermore, BAPTA-AM pretreatment remarkably reversed MAM-induced cell death (Fig. 4C). While EGTA, an impermeable Ca^{2+} chelating agent, and Ca^{2+} free medium failed to do so (Supplementary Figs. 3B, 3C, 3D and 3E). MAM induced calcium-calmodulin dependent protein kinase II (CaMKII) phosphorylation in a time-dependent manner (Fig. 4E). KN93, a CaMKII inhibitor, significantly reversed MAM-induced cell death (Fig. 4F). These results indicated that O_{2^-} triggered cytosolic Ca^{2+} accumulation mediated MAM-induced cell death.

3.6. MAM-induced programmed necrosis via Ca^{2+} mediated JNK1/2 activation

A rapid activation of JNK1/2 as early as 0.5 h after MAM treatment and lasted for at least 2 h (Fig. 5A). JNK1/2 inhibitor SP600125 pretreatment significantly reversed MAM-induced cell death (Fig. 5B). Furthermore, NAC and BAPTA-AM pretreatment could abolish MAM-induced JNK1/2 phosphorylation (Fig. 5C and D). However, SP600125 showed no effect on O_{2^-} generation (Fig. 5E) and Ca^{2+} accumulation induced by MAM (Fig. 5F). These results suggested that Ca^{2+} accumulation induced-JNK1/2 activation mediated MAM-induced cell death.

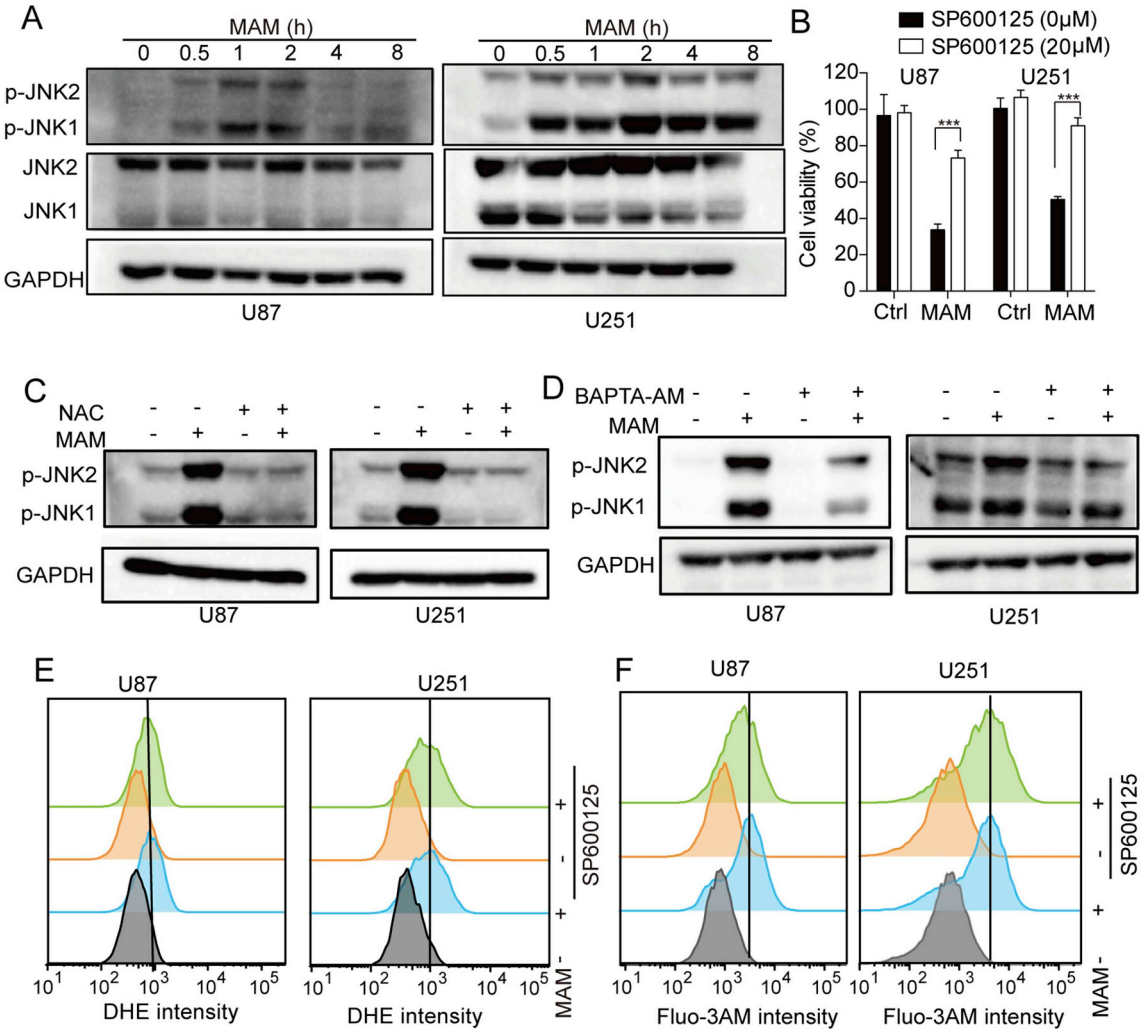

Fig. 5. Sustained JNK1/2 activation triggered by Ca^{2+}. (A) Western blotting analysis evaluating the activation of JNK1/2 in MAM treated cells for different time. GAPDH is used as a loading control. (B) Effect of JNK1/2 inhibitor SP600125 on MAM induced cell death. Cells were treated with MAM for 8 h in the presence or absence of SP600125 pretreatment for 1 h, and then cell viability was determined by MTT assay. Error bars represent standard deviations of the separate experiments. ***$p < 0.001$, analyzed by one-way ANOVA with Dunnett's *post hoc* test. (C and D) Effect of NAC and BAPTA-AM on the activation of JNK1/2 by Western blotting analysis. Cells were pretreated with NAC or BAPTA-AM for 1 h, and then exposure with MAM for another 1 h. (E and F) Effect of SP600125 on MAM-induced O_{2^-} generation (E) and Ca^{2+} accumulation (F). Cells were treated with MAM for 4 h or 8 h in the presence or absence of SP600125 pretreatment for 1 h, followed by DHE staining or Fluo-3AM and flow cytometry analysis.

3.7. MAM-induced programmed necrosis involved mitochondrial dysfunction

MitoTracker staining showed that mitochondria became fragmented into small dots scattered throughout the cell after MAM treatment for 1–2 h. Intracellular big bubbles were observed after MAM treatment for 4 h and penetration of PI was observed after MAM treatment for 8 h (Fig. 6A). MAM induced severe ΔΨm collapse as determined by JC-1 and TMRM staining, which could be significantly prevented by pretreatment of DIC, catalase, SP600125, and BAPTA-AM (Fig. 6B and C). MitoSox Red results showed that MAM induced a large amount of mitochondrial O_{2^-} generation, which could be significantly prevented by pretreatment of DIC, catalase, SP600125, or BAPTA-AM (Fig. 6D). Thus, these results indicated the involvement of mitochondrial dysfunction in MAM-induced programmed necrosis.

3.8. MAM inhibited glioma in zebrafish xenograft model

In U251-derived xenograft zebrafish model, MAM treatment dramatically inhibited tumor growth at 3 days after injection. The inhibitory effect of MAM at 50 nM was comparable to that of TMZ at 100 μM (Fig. 7A and B). No cleavage of caspases 3, 7, and 8 was observed (Fig. 7C). In contrast, increased phosphorylation of JNK1/2 and HMGB1 were detected.

4. Discussion

We previously reported the anticancer effects and mechanisms of MAM in lung, breast, and colon cancers [16–18]. Here, we investigated the anticancer effect of MAM in GBM cells. The main findings of this study included: (1) MAM is a bioactive substrate of NQO1. (2) MAM triggered an NQO1 dependent non-apoptotic necrosis mediated by O_{2^-}/Ca^{2+}/JNK1/2. (3) MAM inhibited malignant glioma growth *in vivo*.

Our data mining results were consistent with previous reports that the expression of NQO1 in numerous solid tumors, including glioma, was increased [14,30–32]. Especially, we found that NOQ1 expression in GBM specimens was positively related to the degree of malignancy. As NQO1 has been considered as a potential target for cancer therapy [33,34], GBM might be the cancer type of interest.

The cytotoxic effect of MAM as evaluated by MTT, ATP, and colony

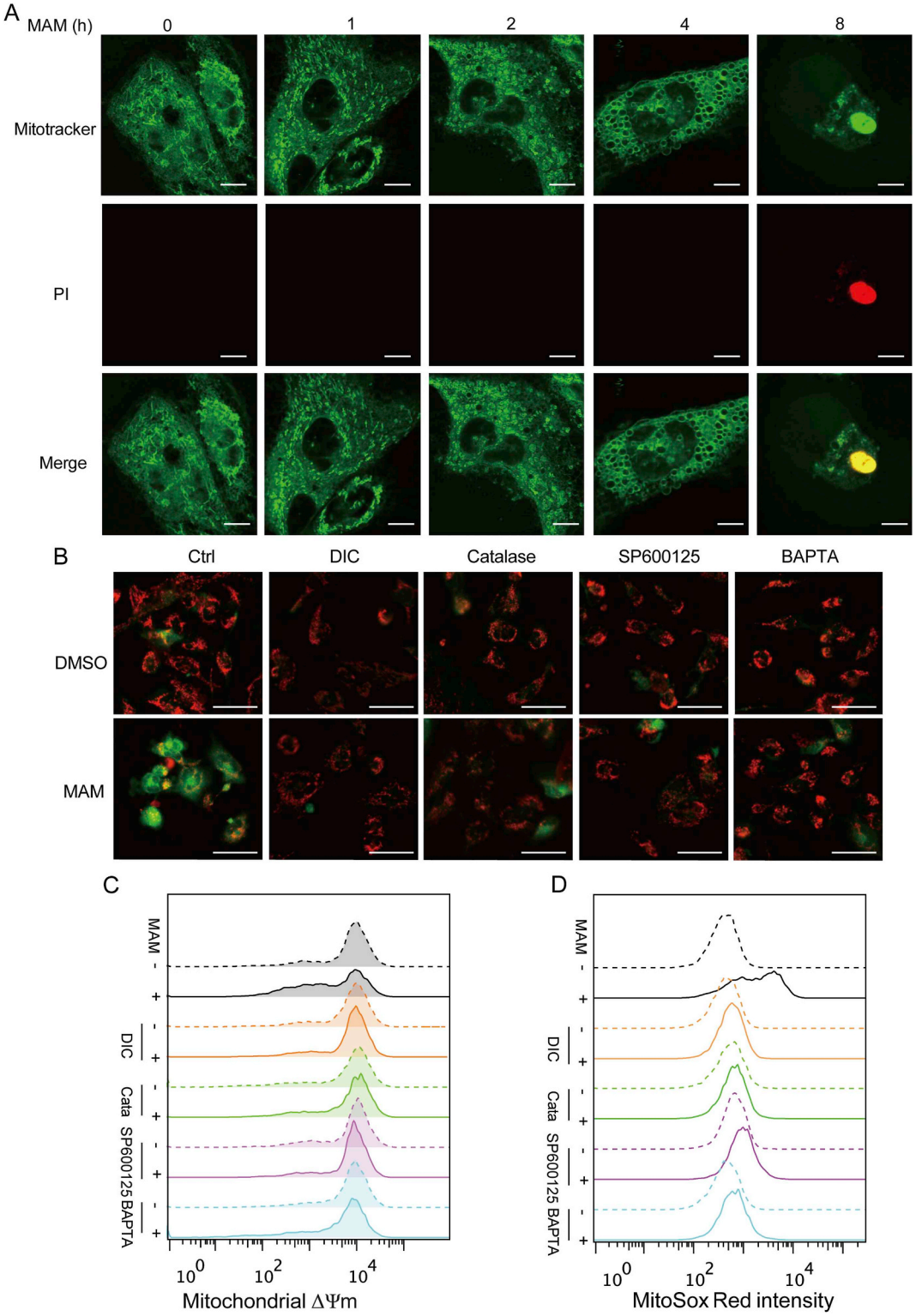

Fig. 6. Involvement of mitochondrial dysfunction in MAM-induced cell death in GBM cells. (A) U251 cells were treated with MAM for the indicated time points followed by Mitotracker (5 μM) and PI staining and then captured by Leica SP8 inverted confocal microscope. Bar = 10 μm. (B) U251 cells were treated with MAM for 4 h with or without pretreatment of various inhibitors (DIC, catalase, SP600125, BAPTA-AM) for 1 h, followed by JC-1 staining. Images were captured with an IN Cell Analyzer 2000. Bar = 50 μm. (C and D) U251 cells were pretreated with various inhibitors (DIC, catalase, SP600125, BAPTA-AM) for 1 h, followed by MAM insult for another 4 h. Cells were stained with mitochondrial potential probe TMRM (C) or MitoSox Red (D) before flow cytometry analysis. Cata: catalase. (For interpretation of the references to colour in this figure legend, the reader is referred to the Web version of this article.)

formation assays showed that it inhibited malignant glioma cells with IC_{50} values at 7.5 μM, which is more effective than TMZ. TMZ kills glioma cells by induction of apoptosis [35,36]. In contrast, MAM treatment showed no effect on caspases 3/7 activities and caspase cleavage. Furthermore, the pan-caspase inhibitor Z-VAD-fmk failed to reverse MAM-induced cell death. Thus, MAM induced non-apoptotic

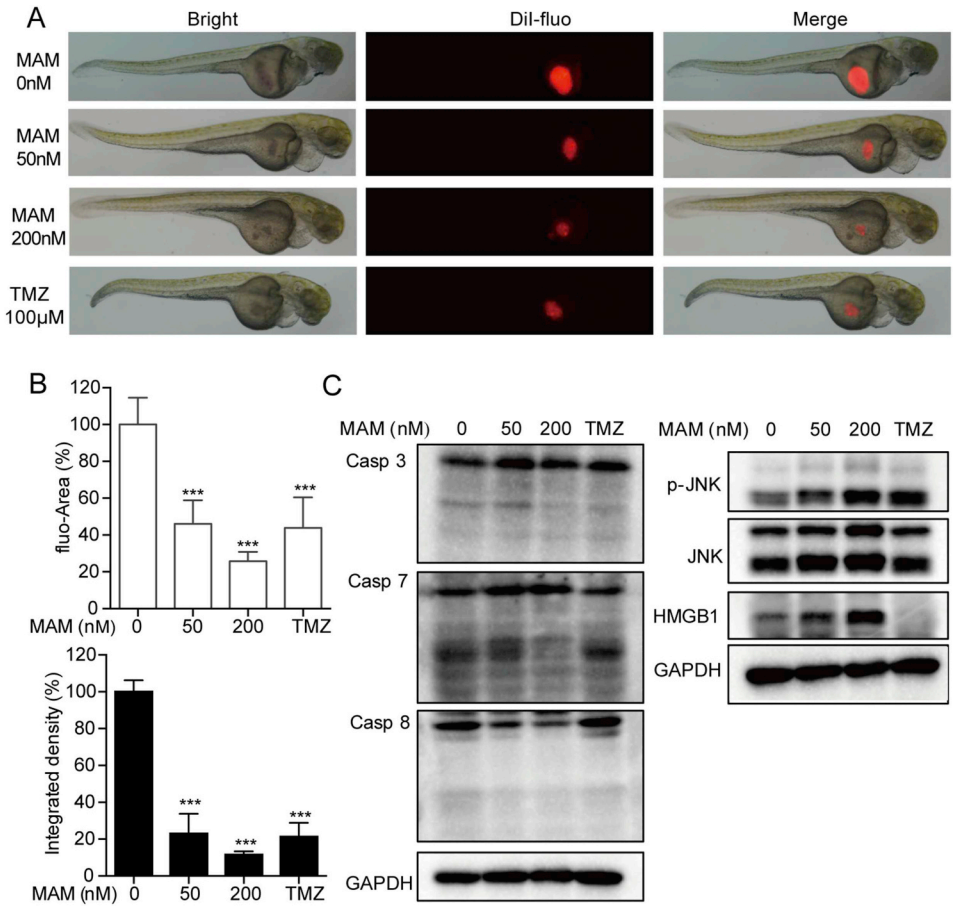

Fig. 7. Anticancer effect of MAM on U251-derived xenograft zebrafish model. (A) The representative image of the tumor-bearing zebrafishes exposed to MAM or TMZ for 2 days. The *in vivo* growth was indicated by red fluorescence. (B) The growth inhibition rates were indicated by fluorescence area and integrated density, calculated as percentage relative to the control values, (n = 8). (C) The expression levels of caspase 3,7, 8, JNK1/2 and HMGB1 in the MAM treated U251-derived xenograft zebrafish were determined by Western blotting analysis. (For interpretation of the references to colour in this figure legend, the reader is referred to the Web version of this article.)

cell death. This was confirmed by Annexin V/7AAD double staining assay. The penetration of PI and increased LDH release revealed the membrane integrity injury. Collectively, these results suggested that MAM induced non-apoptotic necrosis in GBM cells.

Recent research has identified quite a few types of regulated necrosis, such as RIP3/MLKL mediated necroptosis, iron/GPX4/ACSL4 mediated ferroptosis, etc [37,38]. Here, we demonstrated that MAM could directly bind and activate NQO1, suggesting that MAM might preferentially target NQO1. Both NQO1 silence and activity inhibition protected against MAM-induced cell death suggesting that MAM-induced necrosis was NQO1-dependent. The critical role of NQO1 was further confirmed that MAM has no cytotoxicity to NQO1 null H596 cells (Supplementary Fig. 4). Thus, MAM triggered an NQO1-dependent necrosis in GBM cells.

Our previous studies established the critical roles of ROS in MAM-induced cell death in lung cancer, breast cancer, melanoma, and colon cancer cells [16–18]. Here, we further identified that MAM caused a rapid increase of O_{2^-}. ROS scavengers NAC, GSH, catalase, and DTT attenuated MAM induced cell death, indicating the important role of O_{2^-}. The inhibitory effect of MAM-induced O_{2^-} by DIC revealed that the O_{2^-} was caused by NQO1 activation.

Ca^{2+} and JNK1/2 play important roles in various types of programmed cell death [39,40]. MAM-triggered intracellular Ca^{2+} accumulation was confirmed by two methods. MAM-induced cell death was inhibited by the cell-permeant Ca^{2+} chelator BAPTA-AM while EGTA and calcium-free medium failed to do so. This suggested the important role of Ca^{2+} accumulation. Though the exact mechanism of Ca^{2+} increase needs further investigation, it was not from the extracellular import and thus may differ from that of necroptosis. The increased phosphorylation levels of CaMKII and the inhibitory effect of KN93 indicated the involvement of CaMKII in MAM-induced programmed necrosis. We also observed sustained JNK1/2 activation and SP600125, the JNK1/2 inhibitor, significantly inhibited MAM-induced cell death without affecting O_{2^-} generation and Ca^{2+} accumulation. While NAC and BAPTA-AM significantly inhibited MAM-induced JNK1/2 activation. These data suggested that JNK1/2 was the downstream signal of O_{2^-}/Ca^{2+}. Besides, the reversal effects of DIC, catalase, SP600125, and BAPTA-AM on MAM-induced ΔΨm decrease and mitochondria O_{2^-} generation suggested that mitochondria dysfunction might be the final consequence of MAM, resulting in the rapid decrease of cellular ATP levels. Collectively, these *in vitro* results demonstrated that MAM-induced an NQO1 dependent programmed necrosis mediated by O_{2^-}/Ca^{2+}/JNK1/2.

MAM significantly inhibited tumor growth in U251-derived xenograft zebrafish model. Especially, the inhibitory effect at 50 nM was comparable to that of 100 μM TMZ suggesting that MAM was more efficient than TMZ. Furthermore, no-cleavage of caspases and increased expression of JNK1/2 and HMGB1 indicated that the *in vivo* anticancer effect might be apoptosis-independent, which needs further investigation to elucidate.

In conclusion, as depicted in Fig. 8, MAM triggered a non-apoptotic regulated necrosis by targeting NQO1 mediated by O_{2^-}/Ca^{2+}/JNK1/2 in GBM cells. It inhibited tumor growth in a zebrafish xenograft model. Though the therapeutic potentials of MAM for glioma treatment need further investigation, the present study provided a new strategy for fighting glioma by induction of regulated necrosis.

Declaration of competing interest

The authors declare no potential conflicts of interest.

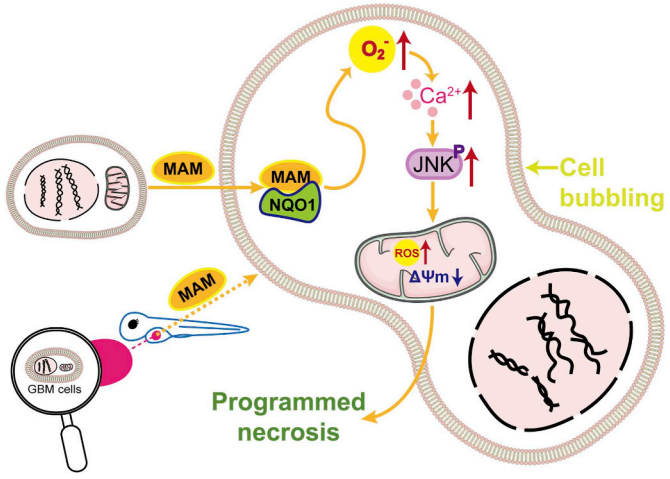

Fig. 8. Schematic representation of the NQO1 mediated programmed necrosis induced by MAM *in vitro* and *in vivo*. MAM triggered NQO1 activation by directly binding and targeting NQO1 and subsequent inducing O_{2^-} production. Ca^{2+} production and JNK1/2 activation functioned as the downstream effector of NQO1 triggered O_{2^-} generation. Mitochondrial dysfunction was the final step of MAM-triggered programmed necrosis. For the *in vivo* effect, MAM inhibited tumor growth in zebrafish xenograft model possibly through the induction of programmed necrosis. ΔΨm, mitochondrial membrane potential; O_{2^-}, superoxide.

Acknowledgments

This work was supported by the Science and Technology Development Fund, Macau S.A.R (FDCT) (078/2016/A2) and the Research Fund of University of Macau (MYRG2016-00043-ICMS-QRCM).

Appendix A. Supplementary data

Supplementary data to this article can be found online at https://doi.org/10.1016/j.freeradbiomed.2020.03.026.

References

[1] R. Chen, A.L. Cohen, H. Colman, Targeted therapeutics in patients with high-grade gliomas: past, present, and future, Curr. Treat. Options Oncol. 17 (8) (2016) 42.
[2] M.C. de Gooijer, N.A. de Vries, T. Buckle, L.C.M. Buil, J.H. Beijnen, W. Boogerd, O. van Tellingen, Improved brain penetration and antitumor efficacy of temozolomide by inhibition of ABCB1 and ABCG2, Neoplasia 20 (7) (2018) 710–720.
[3] A.A. Stavrovskaya, S.S. Shushanov, E.Y. Rybalkina, Problems of glioblastoma multiforme drug resistance, Biochemistry (Mosc.) 81 (2) (2016) 91–100.
[4] D. Ross, D. Siegel, NAD(P)H:quinone oxidoreductase 1 (NQO1, DT-diaphorase), functions and pharmacogenetics, Methods Enzymol. 382 (2004) 115–144.
[5] A.L. Pey, C.F. Megarity, D.J. Timson, NAD(P)H quinone oxidoreductase (NQO1): an enzyme which needs just enough mobility, in just the right places, Biosci. Rep. 39 (1) (2019).
[6] A. Marin, A. Lopez de Cerain, E. Hamilton, A.D. Lewis, J.M. Martinez-Penuela, M.A. Idoate, J. Bello, DT-diaphorase and cytochrome B5 reductase in human lung and breast tumours, Br. J. Canc. 76 (7) (1997) 923–929.
[7] A.M. Malkinson, D. Siegel, G.L. Forrest, A.F. Gazdar, H.K. Oie, D.C. Chan, P.A. Bunn, M. Mabry, D.J. Dykes, S.D. Harrison, et al., Elevated DT-diaphorase activity and messenger RNA content in human non-small cell lung carcinoma: relationship to the response of lung tumor xenografts to mitomycin Cl, Canc. Res. 52 (17) (1992) 4752–4757.
[8] M. Belinsky, A.K. Jaiswal, NAD(P)H:quinone oxidoreductase1 (DT-diaphorase) expression in normal and tumor tissues, Canc. Metastasis Rev. 12 (2) (1993) 103–117.
[9] P. Joseph, T. Xie, Y. Xu, A.K. Jaiswal, NAD(P)H:quinone oxidoreductase1 (DT-diaphorase): expression, regulation, and role in cancer, Oncol. Res. 6 (10–11) (1994) 525–532.
[10] T. Okamura, K. Kurisu, W. Yamamoto, H. Takano, M. Nishiyama, NADPH/quinone oxidoreductase is a priority target of glioblastoma chemotherapy, Int. J. Oncol. 16 (2) (2000) 295–303.
[11] M.A. Silvers, S. Deja, N. Singh, R.A. Egnatchik, J. Sudderth, X. Luo, M.S. Beg, S.C. Burgess, R.J. DeBerardinis, D.A. Boothman, M.E. Merritt, The NQO1 bioactivatable drug, beta-lapachone, alters the redox state of NQO1 + pancreatic cancer cells, causing perturbation in central carbon metabolism, J. Biol. Chem. 292 (44) (2017) 18203–18216.
[12] E.I. Parkinson, P.J. Hergenrother, Deoxynyboquinones as NQO1-activated cancer therapeutics, Acc. Chem. Res. 48 (10) (2015) 2715–2723.
[13] X.M. Huang, Y. Dong, E.A. Bey, J.A. Kilgore, J.S. Bair, L.S. Li, M. Patel, E.I. Parkinson, Y.G. Wang, N.S. Williams, J.M. Gao, P.J. Hergenrother, D.A. Boothman, An NQO1 substrate with potent antitumor activity that selectively kills by PARP1-induced programmed necrosis, Canc. Res. 72 (12) (2012) 3038–3047.
[14] E.A. Bey, M.S. Bentle, K.E. Reinicke, Y. Dong, C.R. Yang, L. Girard, J.D. Minna, W.G. Bornmann, J.M. Gao, D.A. Boothman, An NQO1-and PARP-1-mediated cell death pathway induced in non-small-cell lung cancer cells by beta-lapachone, Proc. Natl. Acad. Sci. U.S.A. 104 (28) (2007) 11832–11837.
[15] D.E. Gerber, M.S. Beg, F. Fattah, A.E. Frankel, O. Fatunde, Y. Arriaga, J.E. Dowell, A. Bisen, R.D. Leff, C.C. Meek, W.C. Putnam, R.R. Kallem, I. Subramaniyan, Y. Dong, J. Bolluyt, V. Sarode, X. Luo, Y. Xie, B. Schwartz, D.A. Boothman, Phase 1 study of ARQ 761, a beta-lapachone analogue that promotes NQO1-mediated programmed cancer cell necrosis, Br. J. Canc. 119 (8) (2018) 928–936.
[16] W. Sun, J.L. Bao, W. Lin, H.W. Gao, W.W. Zhao, Q.W. Zhang, C.H. Leung, D.L. Ma, J.J. Lu, X.P. Chen, 2-Methoxy-6-acetyl-7-methyljuglone (MAM), a natural naphthoquinone, induces NO-dependent apoptosis and necroptosis by H2O2-dependent JNK activation in cancer cells, Free Radical Biol. Med. 92 (2016) 61–77.
[17] W. Sun, X.X. Wu, H.W. Gao, J. Yu, W.W. Zhao, J.J. Lu, J.H. Wang, G.H. Du, X.P. Chen, Cytosolic calcium mediates RIP1/RIP3 complex-dependent necroptosis through JNK activation and mitochondrial ROS production in human colon cancer cells, Free Radical Biol. Med. 108 (2017) 433–444.
[18] W. Sun, J. Yu, H. Gao, X. Wu, S. Wang, Y. Hou, J.J. Lu, X. Chen, Inhibition of lung cancer by 2-methoxy-6-acetyl-7-methyljuglone through induction of necroptosis by targeting receptor-interacting protein 1, antioxidants & redox signaling, (2019).
[19] C.M. Chern, Y.H. Wang, K.T. Liou, Y.C. Hou, C.C. Chen, Y.C. Shen, 2-Methoxystypandrone ameliorates brain function through preserving BBB integrity and promoting neurogenesis in mice with acute ischemic stroke, Biochem. Pharmacol. 87 (3) (2014) 502–514.
[20] P. Tsvetkov, G. Asher, V. Reiss, Y. Shaul, L. Sachs, J. Lotern, Inhibition of NAD(P)H : quinone oxidoreductase 1 activity and induction of p53 degradation by the natural phenolic compound curcumin, Proc. Natl. Acad. Sci. U.S.A. 102 (15) (2005) 5535–5540.
[21] G.S. Oh, H.J. Kim, J.H. Choi, A. Shen, S.K. Choe, A. Karna, S.H. Lee, H.J. Jo, S.H. Yang, T.H. Kwak, C.H. Lee, R. Park, H.S. So, Pharmacological activation of NQO1 increases NAD(+) levels and attenuates cisplatin-mediated acute kidney injury in mice, Kidney Int. 85 (3) (2014) 547–560.
[22] R. Jafari, H. Almqvist, H. Axelsson, M. Ignatushchenko, T. Lundback, P. Nordlund, D.M. Molina, The cellular thermal shift assay for evaluating drug target interactions in cells, Nat. Protoc. 9 (9) (2014) 2100–2122.
[23] T.P. Miettinen, M. Bjorklund, NQO2 is a reactive oxygen species generating off-target for acetaminophen, Mol. Pharm. 11 (12) (2014) 4395–4404.
[24] G. Asher, O. Dym, P. Tsvetkov, J. Adler, Y. Shaul, The crystal structure of NAD(P)H quinone oxidoreductase 1 in complex with its potent inhibitor dicoumarol, Biochemistry 45 (20) (2006) 6372–6378.
[25] G.M. Morris, R. Huey, W. Lindstrom, M.F. Sanner, R.K. Belew, D.S. Goodsell, A.J. Olson, AutoDock4 and AutoDockTools4: automated docking with selective receptor flexibility, J. Comput. Chem. 30 (16) (2009) 2785–2791.
[26] E.F. Pettersen, T.D. Goddard, C.C. Huang, G.S. Couch, D.M. Greenblatt, E.C. Meng, T.E. Ferrin, UCSF chimera - a visualization system for exploratory research and analysis, J. Comput. Chem. 25 (13) (2004) 1605–1612.
[27] C.J. Huang, Y.A. Luo, J.W. Zhao, F.W. Yang, H.W. Zhao, W.H. Fan, P.F. Ge, Shikonin kills glioma cells through necroptosis mediated by RIP-1, PloS One 8 (6) (2013).
[28] X. Chen, J. Wang, Z. Cao, K. Hosaka, L. Jensen, H. Yang, Y. Sun, R. Zhuang, Y. Liu, Y. Cao, Invasiveness and metastasis of retinoblastoma in an orthotopic zebrafish tumor model, Sci. Rep. 5 (2015) 10351.
[29] L. Tian, S.A. Hires, T. Mao, D. Huber, M.E. Chiappe, S.H. Chalasani, L. Petreanu, J. Akerboom, S.A. McKinney, E.R. Schreiter, C.I. Bargmann, V. Jayaraman, K. Svoboda, L.L. Looger, Imaging neural activity in worms, flies and mice with improved GCaMP calcium indicators, Nat. Methods 6 (12) (2009) 875–881.
[30] M. Kanamori, T. Higa, Y. Sonoda, S. Murakami, M. Dodo, H. Kitamura, K. Taguchi, T. Shibata, M. Watanabe, H. Suzuki, I. Shibahara, R. Saito, Y. Yamashita, T. Kumabe, M. Yamamoto, H. Motohashi, T. Tominaga, Activation of the NRF2 pathway and its impact on the prognosis of anaplastic glioma patients, Neuro Oncol. 17 (4) (2015) 555–565.
[31] G. Chakrabarti, M.A. Silvers, M. Ilcheva, Y.L. Liu, Z.R. Moore, X.Q. Luo, J.M. Gao, G. Anderson, L.L. Liu, V. Sarode, D.E. Gerber, S. Burma, R.J. DeBerardinis, S.L. Gerson, D.A. Boothman, Tumor-selective use of DNA base excision repair inhibition in pancreatic cancer using the NQO1 bioactivatable drug, beta-lapachone, Sci. Rep. Uk 5 (2015).
[32] E.T. Oh, J.W. Kim, J.M. Kim, S.J. Kim, J.S. Lee, S.S. Hong, J. Goodwin, R.J. Ruthenborg, M.G. Jung, H.J. Lee, C.H. Lee, E.S. Park, C. Kim, H.J. Park, NQO1 inhibits proteasome-mediated degradation of HIF-1 alpha, Nat. Commun. 7 (2016).
[33] E.T. Oh, H.J. Park, Implications of NQO1 in cancer therapy, BMB Rep. 48 (11) (2015) 609–617.
[34] S.K. Beaver, N. Mesa-Torres, A.L. Pey, D.J. Timson, NQO1: a target for the treatment of cancer and neurological diseases, and a model to understand loss of function disease mechanisms, Biochim. Biophys. Acta Protein Proteonomics 1867 (7–8) (2019) 663–676.
[35] W. Gunther, E. Pawlak, R. Damasceno, H. Arnold, A.J. Terzis, Temozolomide induces apoptosis and senescence in glioma cells cultured as multicellular spheroids, Br. J. Canc. 88 (3) (2003) 463–469.

[36] W.P. Roos, L.F. Batista, S.C. Naumann, W. Wick, M. Weller, C.F. Menck, B. Kaina, Apoptosis in malignant glioma cells triggered by the temozolomide-induced DNA lesion O6-methylguanine, Oncogene 26 (2) (2007) 186–197.
[37] Y. Gong, Z. Fan, G. Luo, C. Yang, Q. Huang, K. Fan, H. Cheng, K. Jin, Q. Ni, X. Yu, C. Liu, The role of necroptosis in cancer biology and therapy, Mol. Canc. 18 (1) (2019) 100.
[38] B. Hassannia, P. Vandenabeele, T. Vanden Berghe, Targeting ferroptosis to iron out cancer, Canc. Cell 35 (6) (2019) 830–849.
[39] D.N. Dhanasekaran, E.P. Reddy, JNK-signaling: a multiplexing hub in programmed cell death, Genes Canc. 8 (9–10) (2017) 682–694.
[40] M. Nomura, A. Ueno, K. Saga, M. Fukuzawa, Y. Kaneda, Accumulation of cytosolic calcium induces necroptotic cell death in human neuroblastoma, Canc. Res. 74 (4) (2014) 1056–1066.